creative commons
COMMONS DEED

저작자표시-비영리-변경금지 2.0 대한민국

이용자는 아래의 조건을 따르는 경우에 한하여 자유롭게

- 이 저작물을 복제, 배포, 전송, 전시, 공연 및 방송할 수 있습니다.

다음과 같은 조건을 따라야 합니다:

저작자표시. 귀하는 원저작자를 표시하여야 합니다.

비영리. 귀하는 이 저작물을 영리 목적으로 이용할 수 없습니다.

변경금지. 귀하는 이 저작물을 개작, 변형 또는 가공할 수 없습니다.

- 귀하는, 이 저작물의 재이용이나 배포의 경우, 이 저작물에 적용된 이용허락조건을 명확하게 나타내어야 합니다.
- 저작권자로부터 별도의 허가를 받으면 이러한 조건들은 적용되지 않습니다.

저작권법에 따른 이용자의 권리는 위의 내용에 의하여 영향을 받지 않습니다.

이것은 이용허락규약(Legal Code)을 이해하기 쉽게 요약한 것입니다.

Disclaimer

dCollection

Master's Thesis
석사 학위논문

High performance Organic Photodiode with Wide Linear Dynamic Range: The Role of Crystalline Orientation

Hyunki Ko(고 현 기 高 鉉 基)

Department of
Energy Science & Engineering

DGIST

2021

Master's Thesis
석사 학위논문

High performance Organic Photodiode with Wide Linear Dynamic Range: The Role of Crystalline Orientation

Hyunki Ko(고 현 기 高 鉉 基)

Department of
Energy Science & Engineering

DGIST

2021

High performance Organic Photodiode with Wide Linear Dynamic Range: The Role of Crystalline Orientation

Advisor: Professor Jongmin Choi
Co-advisor: Professor Chiyoung Park

by

Hyunki Ko
Department of Energy Science & Engineering
DGIST

A thesis submitted to the faculty of DGIST in partial fulfillment of the requirements for the degree of Master of Science in the Department of Energy Science & Engineering. The study was conducted in accordance with Code of Research Ethics[1]

11. 03. 2020

Approved by

Professor Jongmin Choi (signature)
(Advisor)

Professor Chiyoung Park (signature)
(Co-Advisor)

[1] Declaration of Ethical Conduct in Research**:** I, as a graduate student of DGIST, hereby declare that I have not committed any acts that may damage the credibility of my research. These include, but are not limited to: falsification, thesis written by someone else, distortion of research findings or plagiarism. I affirm that my thesis contains honest conclusions based on my own careful research under the guidance of my thesis advisor.

High performance Organic Photodiode with Wide Linear Dynamic Range: The Role of Crystalline Orientation

Hyunki Ko

Accepted in partial fulfillment of the requirements for the degree of Master of Science.

11. 16. 2020

Head of Committee Prof. Jongmin Choi (signature)

Committee Member Prof. Chiyoung Park (signature)

Committee Member Prof. Ju Hyuck Lee (signature)

MS/ES
201900000

고 현 기. Hyunki Ko. High performance Organic Photodiode with Wide Linear Dynamic Range: The Role of Crystalline Orientation. Department of Energy Science & Engineering. 2020. 70p. Advisors Prof. Jongmin Choi, Co-Advisors Prof. Chiyoung Park

ABSTRACT

A new polymeric semiconductor, which can effectively extend linear dynamic ranges (LDRs) of organic photodiodes (OPDs), was developed. Copolymers based on alkylthio-substituted benzo[1,2-b:4,5-b']dithiophene (BDT) are synthesized in conjunction with fluorinated terthiophene (BDT-Th-3T) or alkylterthiophene (BDT-Th-3AT). When deposited onto an ITO/polyethylenimine ethoxylated (PEIE) substrate, both copolymer thin films render apparent face-on orientations as indicated in two-dimensional grazing incidence X-ray diffraction (2D-GIXD) results, and especially among them, BDT-Th-3T thin films show much improved crystalline properties. This is because the molecular structure of BDT-Th-3T shows a higher molecular planarity induced by non-covalent intramolecular interaction and small steric hindrance, which are proved from UV-Vis-NIR absorption and Raman spectroscopy studies, respectively. BDT-Th-3T polymers effectively maintain their crystalline properties when are blended with non-fullerene acceptors and form a bulk heterojunction (BHJ) of a percolating network composed of face-on-oriented donors and acceptors, which is favorable for charge carrier transports in a vertical direction of the device. As a result, the optimized OPD shows a high specific detectivity over 1013 jones and an unprecedentedly wide LDR of 232 dB. It is demonstrated that the wide LDR is originated from high charge transporting property of the polymer, which induces a high saturation photocurrent of BHJ.

Keywords: organic photodiode, linear dynamic range, optoelectronic device, thin film, mobility

List of Contents

List of Tables

List of Figures

Figure S5. Noise current spectra of optimized device with (a) BDT-Th-3T (b) BDT-Th-3AT.

Figure S6. Dark *I-V* characteristics of single-carrier devices based on BDT-Th-3T:ITIC and BDT-Th-3AT:ITIC BHJ films. Lines are fittings in the space-charge-limited current regime. The device structure of hole-only is ITO/PEDOT:PSS/BHJ/MoO_3/Ag and electron-only is ITO/PEIE/BHJ/LiF/Al.

Figure S7. *J-V* characteristics of the OPDs based on BDT-Th-3T:ITIC blend films for active layer thickness under the dark and illuminated (620-nm, 1.03×10^{-4} W cm^{-2}) conditions. The devices were thermal annealed at 140°C

I. Introduction

Organic image sensors based on organic semiconductors have a lot of advantages compared with Si image sensors because high absorption coefficients of organic semiconductors enable organic photodiodes (OPDs) to form a very thin active layer in the range of 100-1000 nm.[1-4] Such thin active layers significantly reduce an optical path when the OPD is introduced as a pixel in the image sensor and thus, remarkably suppresses an optical crosstalk phenomenon between neighboring pixels.[5-7] Therefore, tremendous research efforts have been devoted to enhancing the performance of OPDs by designing new diode architectures or developing new semiconductors and hole- and electron-blocking layers, resulting in high specific detectivity values, the figure-of-merits for OPDs, of over 10^{13} Jones. Nevertheless, the inherently low charge carrier mobility of organic semiconductors compared to Si materials inevitably often leads to a low linear dynamic range (LDR) of the OPDs.8 The LDR is the light intensity range where the responsivity is maintained as a constant, and it can be calculated by

$$\mathrm{LDR} = 20\log_{10}(j_{max}/j_{min})\ or\ 20\log_{10}(P_{max}/P_{min}) \qquad (1)$$

where j_{max}/j_{min} and P_{max}/P_{min} are the maximum and minimum values of detectable photocurrent and incident light intensity, respectively. A wide LDR means that the OPD exhibits a constant photoelectric conversion efficiency over a wide range of incident light intensities. For example, if the LDR is sufficiently wide, a clear image without bloom or dark spots can be captured from dark nights to sunny days. Unfortunately, OPDs suffer from a limited LDR (< 200 dB), which is apparently narrower than that of Si-PDs (~240 dB).[9,10] This is because of the correlation between charge carrier mobility and maximum current measurable from OPD, expressed as follows:

$$j_{max} \approx \frac{\varepsilon_P \varepsilon_0 \mu V^2}{d_p^3} \qquad (2)$$

Here, ε_P is the relative permittivity of the polymer, μ is the mobility of the slower charge carrier, and d_p is the thickness of the polymer layer.[11] Therefore, maximum measurable light power density which is in linear relation with photocurrent is also limited by low charge carrier mobility of organic semiconductors, especially in a vertical direction (typically reported as 10^{-5} to 10^{-3} $cm^2\ V^{-1}\ s^{-1}$). As a result, most OPDs show saturation behavior in dynamic range at the power density of ~0.01 W cm^{-2}.[11-18] Therefore, the key to enhance the LDR of OPDs is to increase the vertical mobility of its constituting organic semiconductors.

The charge carrier mobilities of organic semiconductors can be increased by improving interconnected charge carrier pathways in the material aggregates.[19] Therefore, the key for designing high-mobility polymers is

to minimize unfavorable molecular disordering within the aggregates by enhancing effective regular short-range intermolecular aggregation. Therefore, it is speculated that a high level of backbone coplanarity is an important design principle in realizing a high charge carrier mobility for polymer semiconductors; in fact, recent studies indicated that a 2D-like planar backbone typically leads to better crystalline perfectness and thus, a high charge carrier mobility.[20] The planarity of backbones can be ensured by a minimal steric overlap between the substituents on the adjacent carbon atoms. Non-covalent interactions induced by fluorine substitution, such as F···H, F···S, and F···π, can also exert molecular planarity and strong crystalline properties of fluorinated polymers in a thin film.[21-23] In addition, because polymeric semiconductors must be mixed with acceptor molecules in OPD applications, the formation of successful percolation pathways for both charge carriers is another primary requirement for a high charge carrier mobility.[24,25]

In this regard, a 4,8-bis(thiophen-2-yl)benzo[1,2-b:4,5-b´]dithiophene (BDT-Th) moiety is the most appropriate candidate for conjugated polymers as it can simultaneously satisfy forming 2D-like molecular structures and percolating networks with electron-accepting molecules such as 3,9-bis(2-methylene-(3-(1,1-dicyanomethylene)-indanone))-5,5,11,11-tetrakis(4-hexylphenyl)-dithieno[2,3-d:2',3'-d']-s-indaceno[1,2-b:5,6-b']dithiophene (ITIC).[26] A fluorinated terthiophene moiety is strategically introduced in the repeating unit to maximize intermolecular π-π interactions. Furthermore, the 2D-like planarity of BDT-Th can lead to strong van der Waals interactions between the rigid backbone and substrate surface, resulting in a preferential face-on orientation of the polymers.[20, 27-31] Therefore, in this study, we designed and synthesized BDT-Th-based copolymers in conjunction with fluorinated terthiophene units, where BDT-Th-3AT has an alkyl side chain in the terthiophene unit and BDT-Th-3T does not. This could affect the miscibility of the polymer with the acceptor, and we can fine-tune the BHJ morphology. We introduced ITIC as an acceptor considering its complementary absorption to polymers, good thermal stability, suitable energy levels, and planar molecular geometry. Co-facial π-π interactions of 2D-like BDT-polymers may guide 2D-like ITIC molecules to adopt a similarly oriented alignment, thus leading to a BHJ morphology consisting of both face-on oriented donor and acceptor molecules. From UV-Vis-NIR absorption and Raman spectroscopy studies, we demonstrated that both polymers have apparent coplanar geometry, while the 2D-like feature is more highlighted in BDT-Th-3T. The microcrystalline information of the polymers was studied using two-dimensional grazing incidence X-ray diffraction (2D-GIXD), revealing that the synthesized polymers had a self-assembled preferential face-on orientation with a low paracrystalline disorder even after blending with ITIC. With the 2D-crystalline properties, the percolation network structure of the BDT-Th-3T BHJ film enables effective charge transport of holes and electrons in a vertical

direction of the device, resulting in a high specific detectivity and an unprecedentedly high LDR of the OPD.

II. Results and Discussion

Figure 1(a) shows the UV-Vis-NIR absorption spectra for the BDT-Th-3T and BDT-Th-3AT polymer solutions in chloroform. The maximum absorption (λ_{max}) for BDT-Th-3AT and BDT-Th-3T were located at approximately 450 and 560 nm, respectively. An interesting note is that BDT-Th-3T exhibited a significantly red-shifted absorption profile compared with BDT-Th-3AT, which implies that BDT-Th-3T formed aggregates in the solution. In other words, BDT-Th-3AT has much better solubility owing to further introduced alkyl groups in the thiophene.

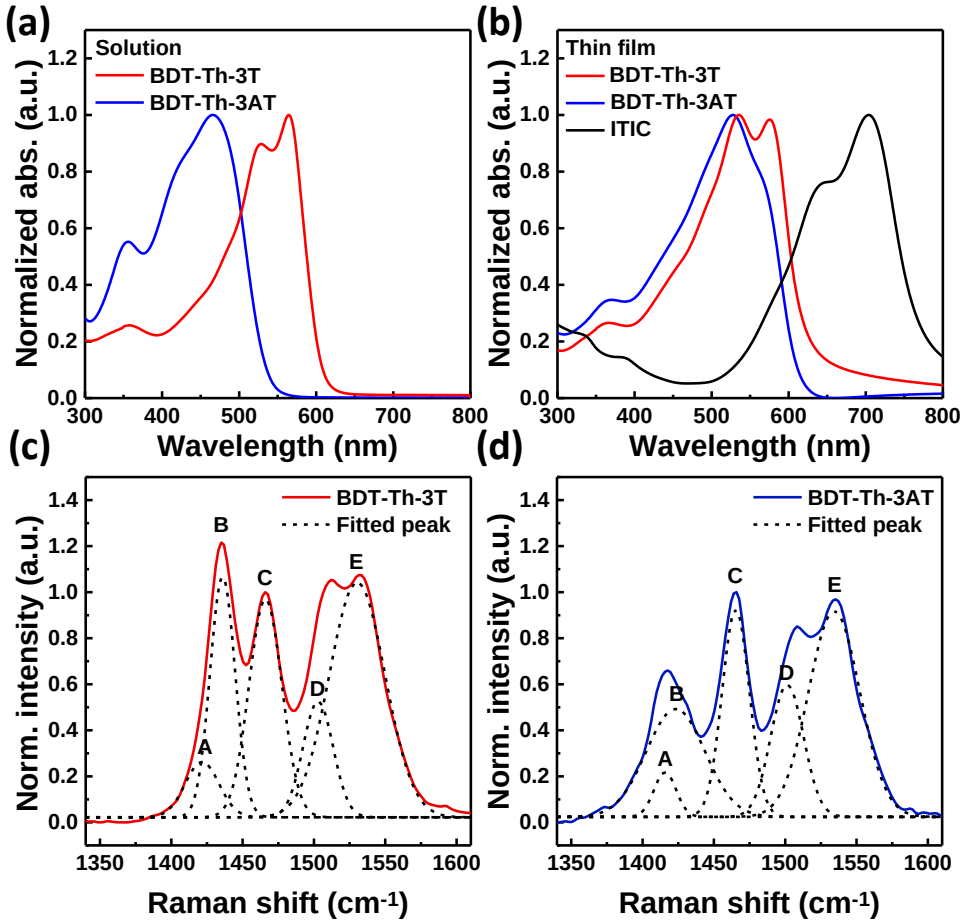

Figure 1. (a-b) Normalized UV-Vis-NIR absorption spectra of the BDT-Th-3T, BDT-Th-3AT, ITIC in (a) solution and (b) thin film state. (c-d) Peak fitting to Raman spectra (532-nm excitation) for neat thin films of (c) BDT-Th-3T and (d) BDT-Th-3AT. In both cases, intensities were normalized with respect to the 1465 cm^{-1} peak intensity. The deconvolved peaks using the Gaussian function are added for the reader's convenience.

Figure 1(b) summarizes their corresponding thin film absorption spectra without thermal annealing. The absorption spectrum of BDT-Th-3AT demonstrated a prominent red shift in the absorption maximum with respect to the solution spectrum, while BDT-Th-3T exhibited only a negligible red shift with the same λ_{max} between the solution and spin-coated film.[32] This result also supports the observation that BDT-Th-3T has a

strong aggregation of the polymer chains in the solution.[19] Another important difference between the two polymers is that only BDT-Th-3T exhibited both distinct 0-0 and 0-1 vibronic features, which is indicative of the rearrangement of the polymer backbone for better crystalline ordering.[20] Collectively, these results indicate that BDT-Th-3T has better crystalline ordering both in solution and solid phases, presumably owing to a more planar backbone conformation originating from a lower steric hindrance and non-covalent interactions within the terthiophene unit. In addition, considering the complementary absorption properties of ITIC, we could expect panchromatic absorption spectra when blending these polymers with ITIC. To get further insight into the effect of the molecular structure on the backbone planarity of polymers, we conducted Raman spectroscopy analysis under a 532 nm laser excitation.

Table 1. Deconvolved Raman Peak Position and Assignment of Each Peak Shown in Figure 1.

	BDT-Th-3T [cm^{-1}]	BDT-Th-3AT [cm^{-1}]	description
A	1421	1414	C-C stretching mode in ring of thiophene
B	1436	1423	C=C stretching of thiophene(delocalized)
C	1465	1465	C=C stretching of thiophene(localized)
D	1502	1501	C=C fused thiophene in the BDT
E	1530	1534	BDT phenyl stretch

As shown in Figure 1(c–d), we collected peaks between 1350 and 1600 cm^{-1}. Because the obtained Raman peaks were too close to be distinguished from each other, we deconvolved each peak using a Gaussian function. All the fitted peaks of both polymers were observed at a similar Raman shift because they had the same conjugated backbone structure except for the side alkyl chain. Kim et al. reported the Raman spectra peak assignments of BDT and thiophene conjugated polymer using DFT geometry optimization results.[33-36] Based on references, we can assign peak A, corresponding to 1421 and 1415 cm^{-1}, to a C-C bond in the thiophene rings. Both peaks B and C, between 1423–1470 cm^{-1}, can be assigned to C=C stretching of thiophene rings on the BDT; B and C correspond to more delocalized and localized π- electrons, respectively. The peaks D and E, located at 1501–1502 and 1530–1534 cm^{-1}, respectively, can be assigned to the C=C fused thiophene in the BDT and the stretching mode of the phenyl ring conjugated with the BDT unit, respectively. While overall spectrum features are very similar between the both polymers, a distinct difference is observed in the relative peak intensities of B and C. Evidently, BDT-Th-3T had a relatively higher peak intensity of B compared with C, indicating the existence of a higher portion of delocalized C=C stretching of thiophene, which can also be interpreted as a more

ordered phase in BDT-Th-3T.[35] By contrast, an inversed relative peak intensity of B and C is observed for BDT-Th-3AT, implying that localized C=C stretching prevails, or a more disordered phase occurs in this alkylated polymer. The Raman analysis result suggests that the excited state molecular orbital in BDT-Th-3T is more delocalized on the thiophene units, which implies an increased planarity of the BDT-Th-3T compared with BDT-Th-3AT.

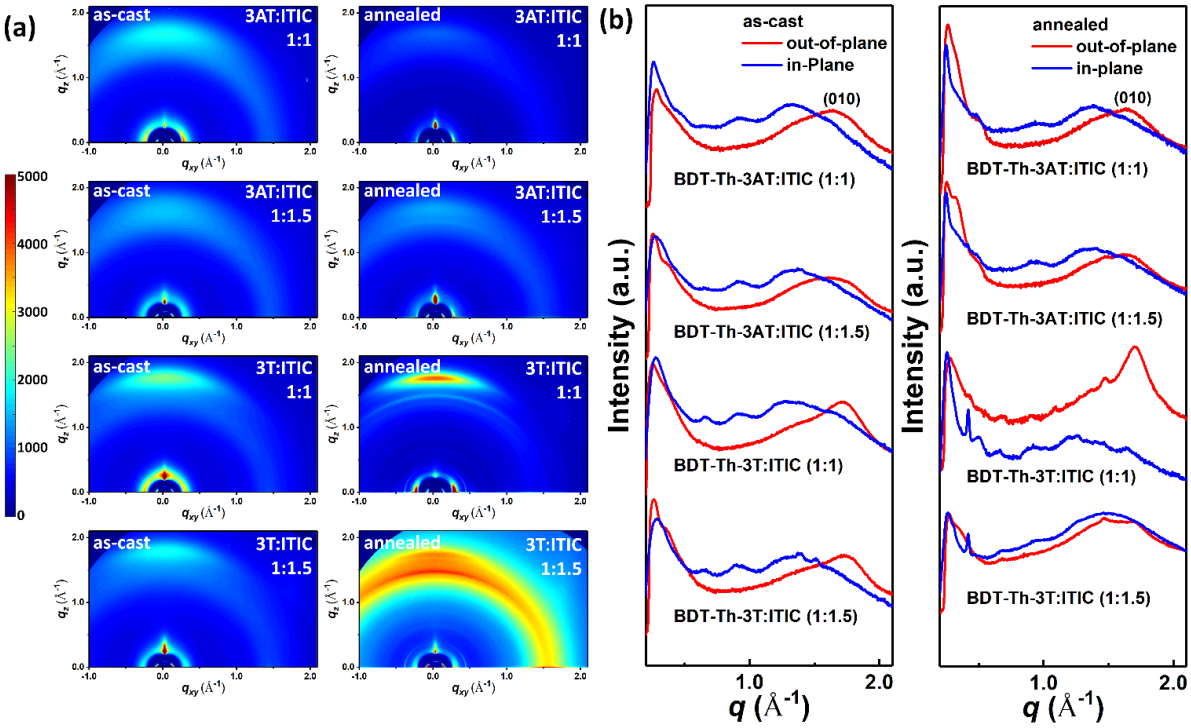

Figure 2. (a) Two-dimensional grazing incidence X-ray diffraction (2D-GIXD) pattern images and (b) their corresponding line-cut profiles of in-plane and out-of-plane directions for BDT-Th-3T:ITIC (1:1 and 1:1.5, wt:wt) blend films and BDT-Th-3AT:ITIC (1:1 and 1:1.5, wt:wt) blend films. The left sides correspond to as-cast films and the right sides correspond to annealed (140 °C) films. The BDT-Th-3T:ITIC (1:1) films exhibit a dominant increase in the intensity of (010) peak, which represents the π-π stacking in face-on direction.

Table 2. Comparison, Based on 2D-GIXD, of Polymer Packing Parameters of The Neat Polymer and Blend Films.

film	$d_{(010)}$ [Å]	q_0[Å]	Δq	$g_{(010)}$ [%]
3AT	3.89	1.613	0.2026	14.14
3T	3.70	1.696	0.1519	11.94
3AT/ITIC (1:1) [a]	3.87	1.622	0.2237	14.88
3AT/ITIC (1:1) [b]	3.86	1.629	0.3190	17.66
3AT/ITIC (1:1.5) [a]	3.93	1.597	0.9651	31.02
3AT/ITIC (1:1.5) [b]	3.89	1.616	0.4229	20.41
3T/ITIC (1:1) [a]	3.68	1.705	0.1678	12.52
3T/ITIC (1:1) [b]	3.70	1.700	0.1202	10.61
3T/ITIC (1:1.5) [a]	3.65	1.721	0.1801	12.91
3T/ITIC (1:1.5) [b]	3.75	1.676	0.2071	14.03

[a]As-cast thin films. [b]Thin films with thermal annealing at 140 °C for 10 min.

We conducted 2D-GIXD analysis to elucidate the microstructure and crystallinity of the neat polymers and their blend films with ITIC and the obtained diffraction images and line-cut profiles are shown in Figure 2 and Figure S3, respectively. All the extracted crystalline parameters are summarized in Table 2. As indicated in Figure S3, BDT-Th-3T without the alkyl chains on the terthiophene has smaller lamellar and co-facial π-π stacking distances of 23.48 and 3.70 Å as revealed by the (001) and (010) peak, respectively, compared with those of BDT-Th-3AT (25.08 and 3.89 Å, respectively) with a linear alkyl chain. For the polymer blend films without thermal annealing, 2D-GIXD showed similar diffraction patterns to those for the neat polymer films, implying that the addition of ITIC did not change the crystalline packing properties of the polymers. On the other hand, after thermal annealing treatment at 140 °C, 1:1 and 1:1.5 (wt:wt) BDT-Th-3T:ITIC blend films exhibited a significantly improved face-on orientation with a significant increase of the (010) peak intensity along the out-of-plane direction. Such change of the polymer crystalline orientation to the preferential face-on orientation is important because it can facilitate vertical charge transport in the OPD device. Interestingly, such a dramatic change of crystalline orientation was not observed from the BDT-Th-3AT blend film. To quantitative estimation of the crystallinity of the polymer films, we calculated the paracrystalline disorder (g) of the (010) peak in the out-of-plane direction.[37] The paracrystalline disorder in the out-of-plane direction is given by

$$g_{(010)} = \sqrt{\frac{\Delta q}{2\pi q_0}} \qquad (3)$$

where Δq is the width of the diffraction peak and q_0 is the center point of the peak. The calculated paracrystalline disorder parameters of the annealed BDT-Th-3T:ITIC are 10.61 and 14.03 for the 1:1 and 1:1.5 blend ratios, respectively. Notably, much higher crystalline disorder parameters of 17.66 and 20.41 were observed from the annealed BDT-Th-3AT:ITIC for the 1:1 and 1:1.5 blend ratios, respectively. The strong face-on orientation with a low paracrystalline disorder observed from the BDT-Th-3T polymer can be due to more planar backbone geometry of the polymer as demonstrated by the UV-Vis-NIR and Raman spectroscopy studies. The well-delocalized π-electrons of BDT-Th-3T would initiate efficient face-to-face interactions with co-facial π-electrons of PEIE in the OPD device, which leading to long-range-ordered face-on orientations of the polymers.[38,39] It is expected that the intermolecular interactions of the planar BDT-Th-3T polymer with the planar ITIC induce a preferential face-on orientation of ITIC in the blend film and this may form an optimal environment of nanoscale percolating pathways for effective hole and electron transports. Actually, GIXD in Figure 2 gives some important clues on this synergetic contribution. GIXD data of neat ITIC as-cast film summarized in Figure S3 showed double diffraction peaks at 0.32 $Å^{-1}$ and 0.42 $Å^{-1}$ in the in-plane direction which can be ascribed to polymorph structure originated from a long alkyl chain of ITIC.[40] Among those, a peak at 0.42 $Å^{-1}$ be-

came more dominant (100) peak of ITIC when blended with polymer as can be seen in Figure 2. Interestingly, when annealed, these (100) peaks of ITIC along with in-plane direction became much sharper especially in the case of BDT-Th-3T blend films compared to those of BDT-Th-3AT, which implies that a preferential face-on orientation of polymer can induce simultaneous face-on orientation of ITIC.

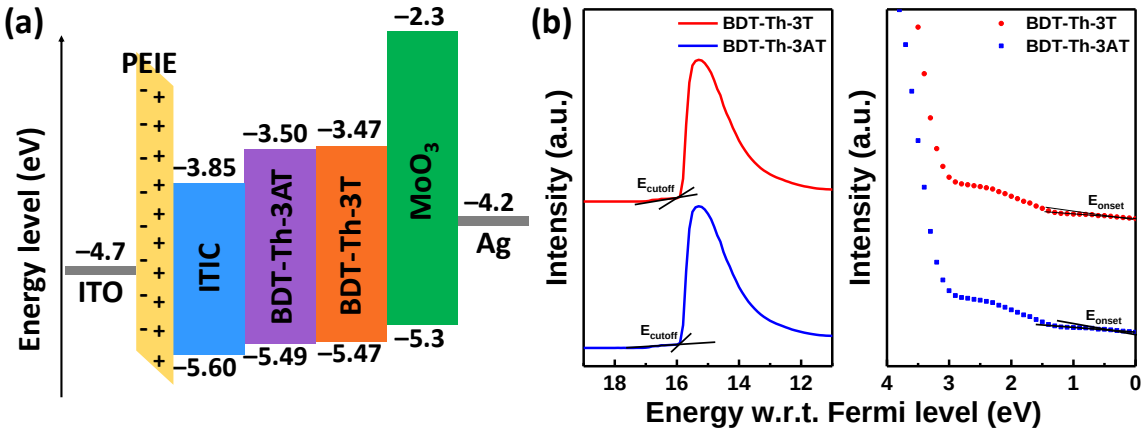

Figure 3. (a) Energy level diagram of the constituting layers of the suggested organic photodiodes (OPDs). The dipole introduced by depositing a thin layer of PEIE reduces the work function of ITO, thus facilitating charge transfer and improving the photocurrent. The highest occupied molecular orbital (HOMO) and lowest unoccupied molecular orbital (LUMO) levels of the BDT-Th-3T and BDT-Th-3AT thin films were calculated by using ultraphotoelectron spectroscopy (UPS) data and optical band gap from thin film absorption spectra. (b) UPS spectra of BDT-Th-3T and BDT-Th-3AT thin films. The HOMO levels are determined by E_{cutoff} which is defined as the high-binding energy cutoff and E_{onset} which is the HOMO level.

We studied OPD properties of the polymers with a diode architecture of ITO/PEIE/BDT-Th-3T or BDT-Th-3AT:ITIC/MoO_3/Ag. The energy level of each layer in the device was noted from either the measurements in this study (for polymer semiconductors) or the reported results. The energy level of each polymer was analyzed using ultraviolet photoelectron spectroscopy (UPS) combined with UV-Vis-NIR absorption spectroscopy. From the UPS spectra in Figure 3(b), the HOMO level of each polymer can be estimated from the secondary cut-off energy. The estimated HOMO levels of BDT-Th-3T and BDT-Th-3AT were 5.47 and 5.49 eV, respectively. In addition, the work function values of both polymers were estimated from the HOMO regions in Figure 3 by measuring the energy distance between the Fermi and HOMO levels. From the onset energy of the HOMO region, the energy distance values between HOMO and work function of both polymers were estimated to be ~0.5 eV, which is typical for p-type conjugated polymer semiconductors. Therefore, as summarized in Figure 3(a), both polymers can form well-defined donor-acceptor junction. PEIE and MoO_3 were optimized as electron transporting (hole blocking) and hole transporting (electron blocking) layers, respectively.

The resulting OPD performances after thermal annealing at 140 °C are summarized in Figure 4. The *J-V* characteristics of non-annealed devices are also summarized in Figure S4 and non-annealed devices showed

slightly lower performances compared with the corresponding devices after annealing due to decreased photocurrent. This result is in good agreement with the 2D-GIXD analyses.

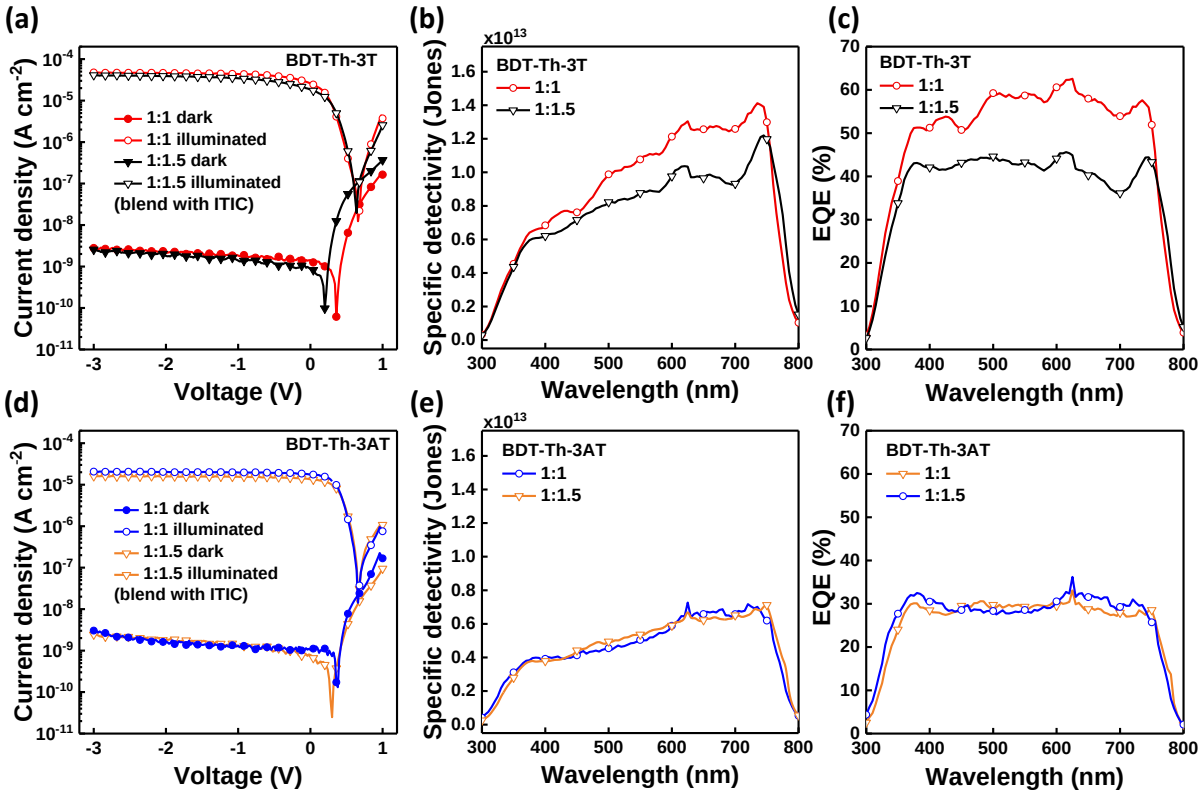

Figure 4. Performances of the optimized OPDs based on BDT-Th-3T:ITIC blend films with thermal treatment at 140 °C. (a) J-V characteristics under the dark and illuminated (620-nm, 1.03×10^{-4} W cm^{-2}) conditions, (b) specific detectivity (D*), and (c) EQE spectra measured under −0.5 V. (d-f) The corresponding performances of the optimized OPDs based BDT-Th-3AT:ITIC blend films. Both cases exhibited a better performance at the blend ratio of 1:1 compared to that of 1:1.5.

The upper and lower panels correspond to BDT-Th-3T and BDT-Th-3AT, respectively. As shown in Figure 4(a) and 4(d), both OPDs exhibited similarly low dark currents of approximately 10^{-9} A cm^{-2} at 0.5 V of reverse bias to each other. However, the BDT-Th-3T:ITIC OPD showed much higher photocurrent particularly for the case of the 1:1 blend ratio. This would be because of the decreased paracrystalline disorder and improved preferential face-on orientation of BDT-Th-3T as confirmed from the 2D-GIXD studies compared to that of BDT-Th-3AT with bulky side alkyl chains. Based on the measured noise current spectrum of each device as shown in Figure S5, specific detectivity spectra were obtained under 0.5 V of a reverse bias using the following equation

$$D^* = \frac{q\lambda\sqrt{A}\cdot\mathrm{EQE}}{hci_{noise}} \qquad (4)$$

where q is the elementary charge, λ is the wavelength of the incident light, A is the photoactive area (0.09 cm^2), EQE is the external quantum efficiency, h is Planck's constant, c is the speed of light, and i_{noise} is the noise cur-

rent.[1] As summarized in Figure 4(b), the OPD with BDT-Th-3T:ITIC (1:1) exhibited extraordinary performance with a peak D^* of 1.4×10^{13} Jones at 740 nm. Such remarkable performance of BDT-Th-3T can be due to its low paracrystalline disorder along with its preferential face-on orientation, which resulting in the percolation pathways for effective charge transport in the ITIC blend film. As shown in Figure 4(c), the EQE of BDT-Th-3T OPD reached a remarkably high value of 62 % at 625 nm, which is much higher than that of BDT-Th-3AT. We measured LDR of the BDT-Th-3T OPD to analyze the effect of the molecular orientation and crystallinity driven by the molecular conformation of the polymer on the dynamic response of OPDs of various light intensities (Figure 5(a)). As estimated from Equation 2, efficient charge separation and collection at each electrode can make a higher upper saturation current of the OPD, thus resulting in a wide LDR. Although thinner thickness of the active layer can be another possible parameter which can enhance LDR according to equation (2), however, as summarized in Figure S6, dark current started to increase exponentially as the active layer thickness became below 300 nm, which should increase lower limit of LDR. As a result, we set 300 nm thickness of the active layer as the optimal condition, which rendered a remarkably high saturation photocurrent of 5 mA at 0.1 W cm^{-2}. Such high value has not been reported from previous OPD studies.[11-18] The lower limit of the LDR can be related to the noise-equivalent power (NEP) of the OPD.

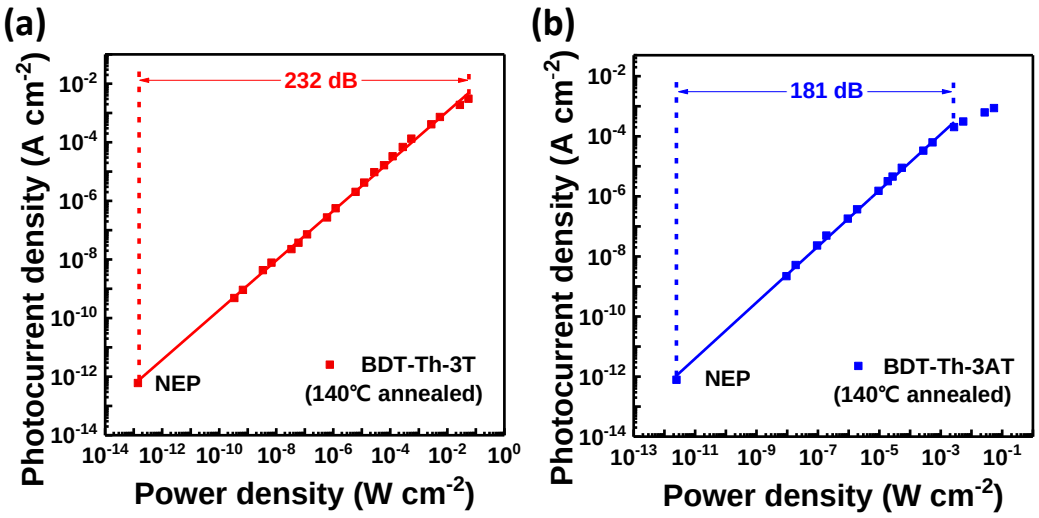

Figure 5. Linear dynamic range (LDR) plots of the optimized OPD measured under −0.5 V fabricated from (a) BDT-Th-3T:ITIC (1:1) and (b) BDT-Th-3AT (1:1) illuminated by monochromatic light source and laser (650-nm wavelength). Deviation from linearity was observed at 55 mW cm^{-2} and 2.7 mW cm^{-2}, which are the upper limits of the LDRs. The lower limit of the LDR is NEP, which is a theoretical value calculated from the noise current. As a result, the optimized OPD based on BDT-Th-3T showed the highest LDR value of 232 dB among other OPDs.

As a result, the optimized device of the BDT-Th-3T:ITIC blend exhibits an unprecedentedly wide LDR value of 232 dB, which is one of the highest values among the recently reported OPDs.[11-18] On the other hand, an ordi-

nary LDR of 181 dB was measured from the BDT-Th-3AT:ITIC blend OPD (Figure 5(b)), implying the importance of the crystalline orientation and perfectness of LDRs. To study the charge carrier transport properties of both blend films along the vertical direction, we conducted space-charge limited current (SCLC) measurements for both hole- and electron-only devices. As shown in Figure S7, electron mobilities of 2.39×10^{-5} and 1.57×10^{-8} cm^2 V^{-1} s^{-1} were calculated from BDT-Th-3T and BDT-Th-3AT, respectively, both of which were lower than their hole mobilities of 5.75×10^{-4} and 1.31×10^{-4} cm^2 V^{-1} s^{-1}, respectively.[41]

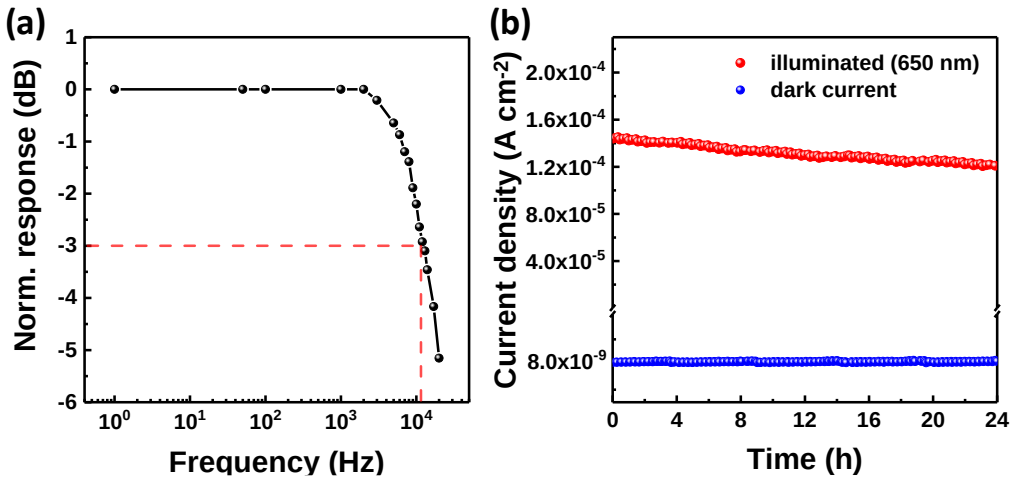

Figure 6. (a) The Bode plot of the optimized OPD (BDT-Th-3T:ITIC (1:1)) to determine –3 dB frequency point under the illumination of red laser (650-nm wavelength, 9.74 mW cm^{-2}). (b) Transient measurement results to show the operating stability of the optimized OPD (BDT-Th-3T:ITIC (1:1)) in terms of both photocurrent and dark current under modulated light signal (650-nm illumination pulsed at 1 Hz, 9.74 mW cm^{-2}). Both measurements were performed at −0.5 V.

Because a slower charge carrier is in charge of the saturation of the photocurrent at a high light intensity, it is expected that the higher electron mobility of the BDT-Th-3T:ITIC blend film enabled such a wide LDR and high specific detectivity. The planar backbone of BDT-Th-3T would induce co-facial interaction of the polymer chain with PEIE, which resulting in a long-range-ordered face-on orientation of the polymer and ITIC. Consequently, this induced effective percolating pathways for both holes and electrons in the bled film, which leading to high OPD performances with a high saturation photocurrent which is essential for a wide LDR.

In the OPD, the rate of response to an external light signal is also very important. In Figure 6(a), the temporal response of the optimized device based on BDT-Th-3T was investigated with increasing the frequency of the external pulsed illumination. The –3 dB cut-off frequency was observed to be 12 kHz, which is a sufficiently rapid value for most video applications.[42] Theoretically, 3 dB frequency (f_{3dB}) can be calculated by the equation

$$f_{3dB}^{-2} = f_t^{-2} + f_{RC}^{-2} \qquad (5)$$

where f_t and f_{RC} are the transit time-limited and RC-limited 3 dB frequencies, respectively.[1] Because slower carrier of the optimized OPD was electron with charge carrier mobility of 2.39×10^{-5} cm^2 V^{-1} s^{-1}, we can calculate

the transit time as 75.3 μs. From the dark *J-V* curve and geometric capacitance, the series resistance and capacitance were calculated as 984 Ω cm^2 and 1.2 nF cm^{-2}, respectively, resulting in 1.26 μs of RC time. Because these transit time and RC time correspond to 7.39 kHz and 131 kHz, respectively, we can guess temporal response of the optimized OPD is transit time-limited. The operating lifetime of the optimized BDT-Th-3T OPD was tested by continuously exposing the device to an external light pulse: a frequency of 1 Hz, light intensity of 9.74 mW cm^{-2}, and wavelength of 650 nm. As shown in Figure 6(b), the OPD exhibited relatively high operating stability for an operation time of 24 h; there was only 10 % reduction in the photocurrent and the dark current was well maintained from the initial performance.

III. Conclusion

A low charge carrier mobility of organic semiconductors has been known to be one of the critical factors which limit LDR of OPDs. In this study, we demonstrated that the narrow LDR of OPDs can be overcome by developing a conjugated polymer that has highly ordered structures with a face-on orientation in a donor:acceptor blend film. As indicated by Raman spectroscopy and 2D-GIXD studies, BDT-Th-3T achieved a remarkably well-arranged face-on orientation with a low paracrystalline disorder even when blended with ITIC due to its highly coplanar backbone geometry. This results in efficient π-electron delocalization on the polymer backbone and thus, a high charge carrier mobility in the vertical direction of the OPD. Consequently, the resulting OPD with an optimized device architecture rendered a high specific detectivity of over 10^{13} Jones, with a wide detection range from 300 to 800 nm and an unprecedentedly wide LDR of 232 dB.

IV. Experimental Section

4.1 Materials

Molybdenum oxide (MoO_3), polyethylenimine ethoxylated (PEIE), 2-methoxyethoanol, chloroform Mucasol, acetone, and isopropanol were purchased from Sigma-Aldrich. 2,2′-[[6,6,12,12-tetrakis(4-hexylphenyl)-6,12-dihydrodithieno[2,3-d:2′,3′-d′]-s-indaceno[1,2-b:5,6-b′]dithiophene-2,8-diyl]bis[methylidyne(3-oxo-1H-indene-2,1(3H)-diylidene)]]bis[propanedinitrile] (ITIC) was purchased from 1-Material and poly(3,4-ethylenedioxythiophene):poly(styrenesulfonate) (PEDOT:PSS; Clevious P VP.Al 4083) aqueous solution was supplied by Heraeus Holding GmbH. All chemicals were used as received without further purification processes.

4.2 Photodiode Fabrication

For the fabrication of OPDs, ITO-patterned glass substrates were cleaned with a series of sequential sonication in Mucasol aqueous solution, distilled water, acetone, and isopropanol. After cleansing processes, the substrates were treated with oxygen plasma to assess hydrophilic properties to the prepared ITO substrate surfaces. The PEIE solution diluted in 2-methoxyethanol with a concentration of 0.35–0.4 wt% was deposited onto the oxygen-plasma-treated ITO substrates in ambient atmospheric conditions by spin-coating at 5000 rpm, followed by the thermal treatment at 100 °C for 10 min, resulting in the film thickness of 5 nm. The BDT-Th-3T and BDT-Th-3AT blend with ITIC ratio of 1:1 and 1:1.5 were dissolved in anhydrous chloroform for the panchromatic absorption OPD, respectively. The blend solutions were spin-coated at 1000 rpm for 30 s on top of the PEIE layers. MoO3/Ag electrodes were deposited onto the ITIC layers by performing sequential thermal evaporation with evaporating rate below 0.5 Å s^{-1}.

4.3 Thin Film Characterization

UV-Vis-NIR absorption spectra were measured using an Agilent Technologies Cary 5000 spectrophotometer. He I excitation source (21.2 eV) was used for UPS measurements. In the UPS experiments, a –5 V bias was applied to the sample to further enhance the collection of the lowest kinetic energy of electrons. 2D-GIXD measurements were performed using the PLS-II 3C and 4D beamline at the Pohang Accelerator Laboratory (PAL) in Korea. All films were manufactured in the same manner that the devices were fabricated.

4.4 Device Characterization

Dark and illuminated J−V characteristics, specific detectivity spectra and EQE spectra were obtained from the combination of an Oriel Cornerstone 130 1/8 m monochromator and Keithley 2450 Sourcemeter, in control of home-made LabView programs. The linear dynamic range was measured by using two different light sources with various optical filters: a monochromator and a laser (650-nm wavelength) whose intensities were less than 103 μW cm^{-2} and up to 55 mW cm^{-2}, respectively. For measuring noise current spectra, a Stanford Research SR830 DSP lock-in amplifier was used in connection with the Keithley 2450 Sourcemeter and a Newport 75160 MHz−kHz Chopper Controller. A TDS5052 digital phosphor oscilloscope (Tektronix) with same laser source was used for measuring –3 dB frequency. All photodiode measurements were performed in a nitrogen-filled glovebox. The thickness of the films was measured by a profilometer (Dektak XT, Bruker).

V. Supporting information

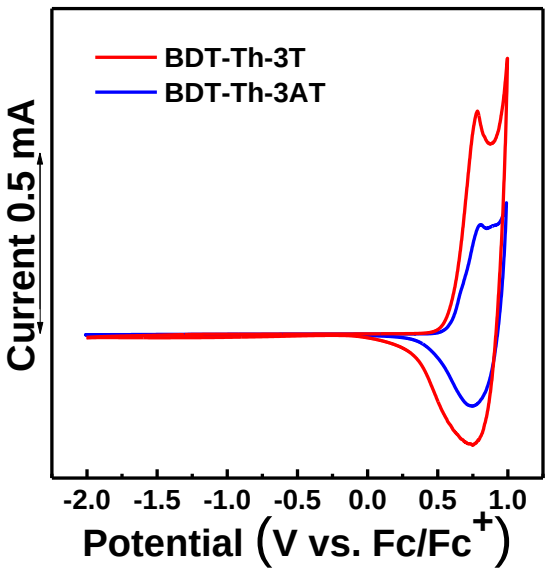

Figure S1. CV curve of the BDT-Th-3T and BDT-Th-3AT.

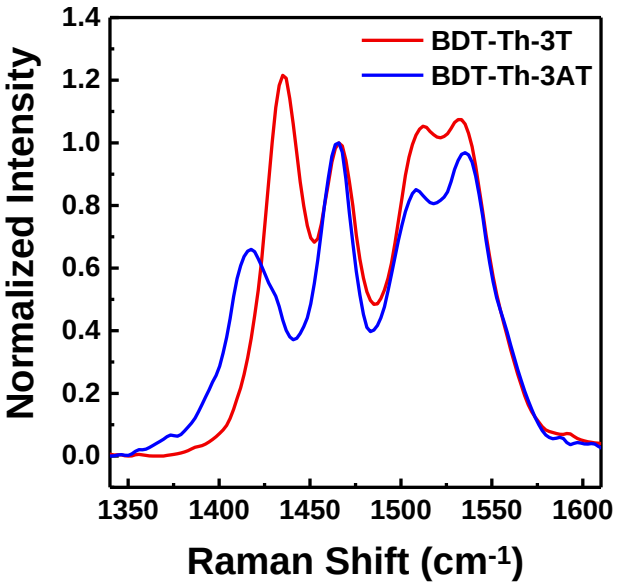

Figure S2. Comparison of Raman spectra for each polymer neat thin films.

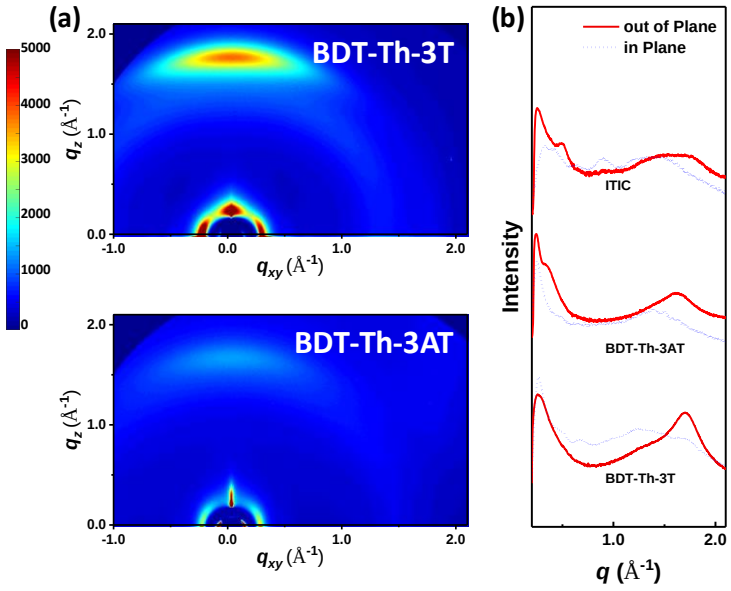

Figure S3. GIXD image and line cut for neat polymer films and ITIC.

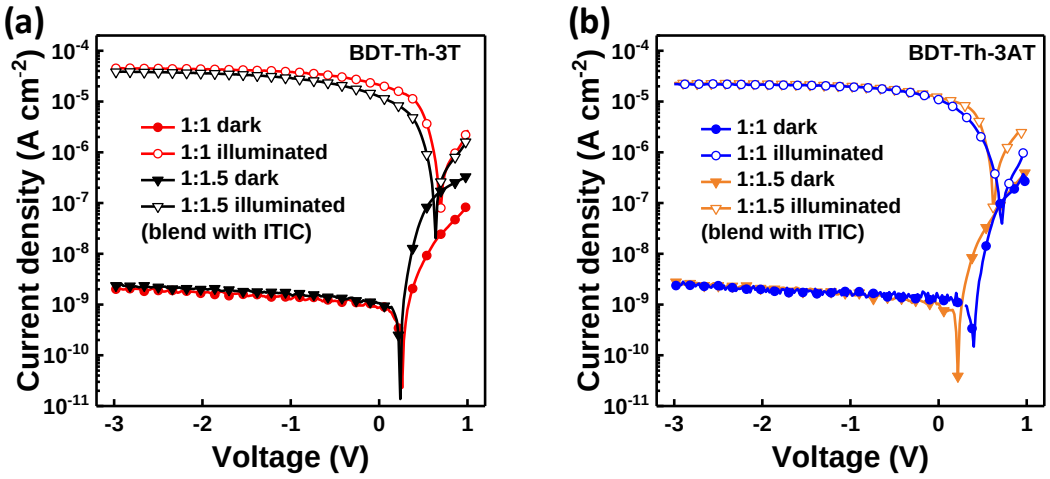

Figure S4. *J-V* characteristic of as-cast device. (a) BDT-Th-3T and (b) BDT-Th-3AT with ITIC, respectively.

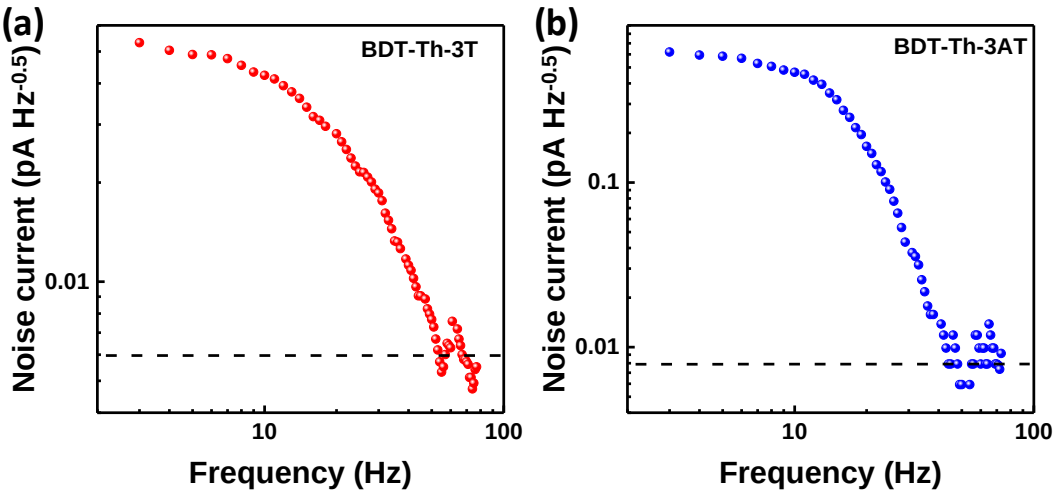

Figure S5. Noise current spectra of optimized device with (a) BDT-Th-3T (b) BDT-Th-3AT.

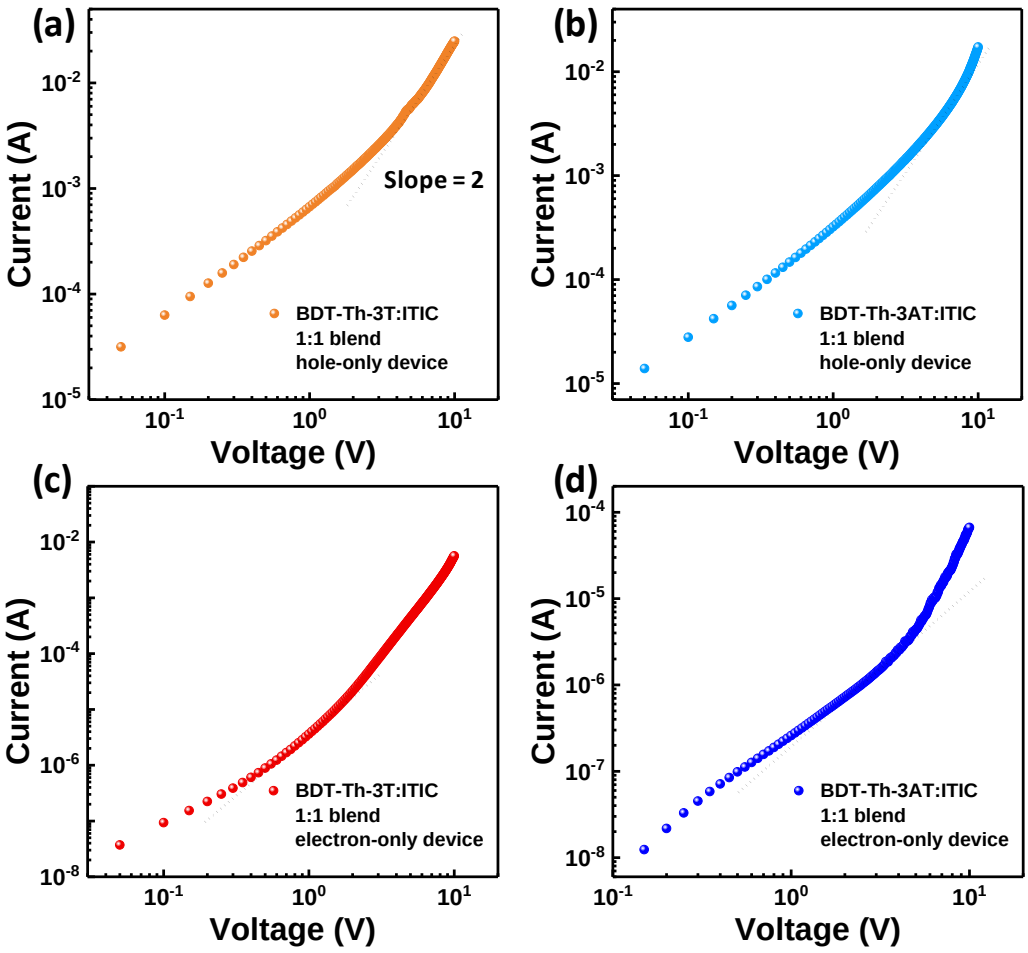

Figure S6. Dark *I-V* characteristics of single-carrier devices based on BDT-Th-3T:ITIC and BDT-Th-3AT:ITIC BHJ films. Lines are fittings in the space-charge-limited current regime. The device structure of hole-only is ITO/PEDOT:PSS/BHJ/MoO_3/Ag and electron-only is ITO/PEIE/BHJ/LiF/Al.

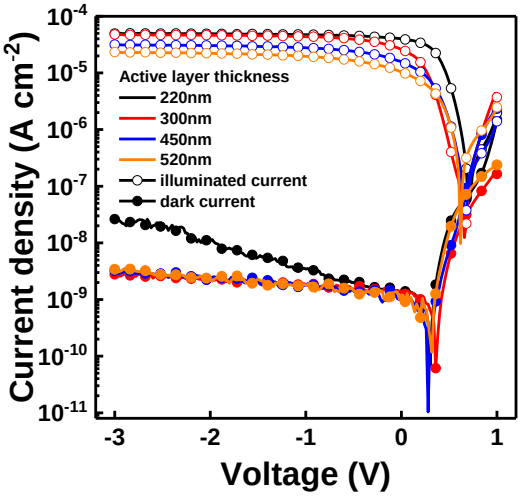

Figure S7. *J-V* characteristics of the OPDs based on BDT-Th-3T:ITIC blend films for active layer thickness under the dark and illuminated (620-nm, 1.03×10^{-4} W cm^{-2}) conditions. The devices were thermal annealed at 140°C

Table S1. UPS values for BDT-Th-3T and BDT-Th-3AT.

polymer	cut-off	onset	homo level
BDT-Th-3T	16.08	0.35	5.47
BDT-Th-3AT	16.11	0.40	5.49

VI. References

[1] Jansen-van Vuuren, R. D.; Armin, A.; Pandey, A. K.; Burn, P. L.; Meredith, P. Organic Photodiodes: The Future of Full Color Detection and Image Sensing. *Adv. Mater*. **2016**, 28, 4766−4802.

[2] Deckman, I.; Lechene, P. B.; Pierre, A.; Arias, A. C. All-printed full-color pixel organic photodiode array with a single active layer. *Org. Electron*. **2018**, 56, 139−145.

[3] Pierre, A.; Deckman, I.; Lechene, P. B.; Arias, A. C. High Detectivity All-Printed Organic Photodiodes. *Adv. Mater*. **2015**, 27, 6411−6417.

[4] Yoon, S.; Sim, K. M.; Chung, D. S. Prospects of Colour Selective Organic Photodiodes. *J. Mater. Chem. C* **2018** , 6, 13084 − 13100.

[5] Li, W.; Li, D.; Dong, G.; Duan, L.; Sun, J.; Zhang, D.; Wang, L. High-stability Organic Red-light Photodetector for Narrowband Applications. *Laser Photonics Rev*. **2016**, 10, 473−480.

[6] Lupton, J.; Koeppe, R.; Müller, J.; Feldmann, J.; Scherf, U.; Lemmer, U. Organic Microcavity Photodiodes. *Adv. Mater*. **2003**, 15, 1471−1474

[7] Armin, A.; Jansen-van Vuuren, R. D.; Kopidakis, N.; Burn, P. L.; Meredith, P. Narrowband Light Detection via Internal Quantum Efficiency Manipulation of Organic Photodiodes. *Nat. Commun*. **2015**, 6, 6343.

[8] Gong, X.; Tong, M.; Xia, Y.; Cai, W.; Moon, J. S.; Cao, Y.; Yu, G.; Shieh, C.-L.; Nilsson, B.; Heeger, A. J. High-Detectivity Polymer Photodetectors with Spectral Response from 300 Nm to 1450 Nm. *Science* **2009**, 325 (5948), 1665−1667

[9] Goto, M.; Honda, Y.; Watabe, T.; Hagiwara, K.; Nanba, M.; Iguchi, Y.; Saraya, T.; Kobayashi, M.; Higurashi, E.; Toshiyoshi, H.; Hiramoto, T. Quarter Video Graphics Array Full-Digital Image Sensing with Wide Dynamic Range and Linear Output Using Pixel-Wise 3D Integration. *IEEE*. **2018**, 1-4.

[10] Simola, E. T.; De Iacovo, A.; Frigerio, J.; Ballabio, A.; Fabbri, A.; Isella, G.; Colace, L. Voltage-tunable dual-band Ge/Si photodetector operating in VIS and NIR spectral range. *Opt Express* **2019**, 27, 8529-8539.

[11] Li, W.; Xu, Y.; Meng, X.; Xiao, Z.; Li, R.; Jiang, L.; Cui, L.; Zheng, M.; Liu, C.; Ding, L.; Lin, Q. Visible to Near-Infrared Photodetection Based on Ternary Organic Heterojunctions. *Adv. Funct. Mater.* **2019**, 29, 1808948.

[12] Armin, A.; Hambsch, M.; Kim, I. K.; Burn, P. L.; Meredith, P.; Namdas, E. B. Thick Junction Broadband Organic Photodiodes. *Laser Photonics Rev.* **2014**, 8, 924−932.

[13] Verstraeten, F.; Gielen, S.; Verstappen, P.; Kesters, J.; Georgitzikis, E.; Raymakers, J.; Cheyns, D.; Malinowski, P.; Daenen, M.; Lutsen, L.; Vandewal, K.; Maes, W. Near-infrared organic photodetectors based on

bay-annulated indigo showing broadband absorption and high detectivities up to 1.1 μm. *J. Mater. Chem. C* **2018**, 6, 11645−11650.

[14] Biele, M.; Montenegro Benavides, C.; Hürdler, J.; Tedde, S. F.; Brabec, C. J.; Schmidt, O. Spray-Coated Organic Photodetectors and Image Sensors with Silicon-Like Performance. *Adv. Mater. Technol.* **2019**, 4, 1800158.

[15] Wang, T.; Wang, Y.; Zhu, L.; Lv, L.; Hu, Y.; Deng, Z.; Cui, Q.; Lou, Z.; Hou, Y.; Teng, F. High Sensitivity and Fast Response Sol-gel ZnO Electrode Buffer Layer based Organic Photodetectors with Large Linear Dynamic Range at Low Operating Voltage. *Org. Electron.* **2018**, 56, 51−58.

[16] Kang, M.; Yoon, S.; Cho, J.; Kim, J.; Chung, D. S. Reactive Dedoping of Polymer Semiconductors To Boost Self-Powered Schottky Diode Performances. *ACS Appl. Mater. Interfaces* **2019**, 11, 8365-8373.

[17] Nie, R.; Deng, X.; Feng, L.; Hu, G.; Wang, Y.; Yu, G.; Xu, J. Highly Sensitive and Broadband Organic Photodetectors with Fast Speed Gain and Large Linear Dynamic Range at Low Forward Bias. *Small* **2017**, 13, 1603260.

[18] Kim, L. K.; Li, X.; Ullah, M.; Shaw, P. E.; Wawrzinek, R.; Namdas, E. B.; Lo, S.-C. High-Performance, Fullerene-Free Organic Photodiodes Based on a Solution-Processable Indigo. *Adv. Mater.* **2015**, 27, 6390−6395.

[19] Kim, N.-K.; Jang, S.-Y.; Pace, G.; Caironi, M.; Park, W.-T.; Khim, D.; Kim, J.; Kim, D.-Y.; Noh, Y.-Y. High-Performance Organic Field-Effect Transistors with Directionally Aligned Conjugated Polymer Film Deposited from Pre-Aggregated Solution. *Chem. Mater.* **2015**, 27 (24), 8345−8353.

[20] Chen, M. S.; Niskala, J. R.; Unruh, D. A.; Chu, C. K.; Lee, O. P.; Frechet, J. M. J. Control of Polymer-Packing Orientation in Thin Films through Synthetic Tailoring of Backbone Coplanarity. *Chem. Mater.* **2013**, 25, 4088-4096.

[21] Reichenbacher, K.; Suss, H. I.; Hulliger, Fluorine in crystal engineering—"the little atom that could". *J. Chem. Soc. Rev.* **2005**, 34, 22

[22] Wang, Y.; Parkin, S. R.; Gierschner, J.; Watson, M. D. Highly Fluorinated Benzobisbenzothiophenes. *Org. Lett.* **2008**, 10, 3307− 3310.

[23] Park, S.; Cho, J.; Ko, M. J.; Chung, D. S.; Son, H. J. Synthesis and Charge Transport Properties of Conjugated Polymers Incorporating Difluorothiophene as a Building Block. *Macromolecules* **2015**, 48, 3883−3889.

[24] Wu, Z.; Yao, W.; London, A. E.; Azoulay, J. D.; Ng, T. N. Temperature-Dependent Detectivity of Near-Infrared Organic Bulk Heterojunction Photodiodes. *ACS Appl. Mater. Interfaces* **2017**, 9, 1654−1660

[25] Eastham, N. D.; Logsdon, J. L.; Manley, E. F.; Aldrich, T. J.; Leonardi, M. J.; Wang, G.; Powers-Riggs, N. E.; Young, R. M.; Chen, L. X.; Wasielewski, M. R.; Melkonyan, F. S.; Chang, R. P. H.; Marks, T. J. Hole-Transfer Dependence on Blend Morphology and Energy Level Alignment in Polymer: ITIC Photovoltaic Materials. *Adv. Mater.* **2017**, 1704263..

[26] Lin, Y.; Wang, J.; Zhang, Z.-G.; Bai, H.; Li, Y.; Zhu, D.; Zhan, X. An Electron Acceptor Challenging Fullerenes for Efficient Polymer Solar Cells. *Adv. Mater.* **2015**, 27, 1170−1174.

[27] Gao, L.; Zhang, Z. G.; Bin, H.; Xue, L.; Yang, Y.; Wang, C.; Liu, F.; Russell, T. P.; Li, Y. High-Efficiency Nonfullerene Polymer Solar Cells with Medium Bandgap Polymer Donor and Narrow Bandgap Organic Semiconductor Acceptor. *Adv. Mater.* **2016**, 28, 8288−8295.

[28] Kim, H. S.; Lee, T. H.; Yeop, J.; Cho, H. W.; Kim, J. W.; Park, S. Y.; Park, J. B.; Kim, J. Y.; Hwang, D.-H. Effect of Substituents of Thienylene−Vinylene−Thienylene-Based Conjugated Polymer Donors on the Performance of Fullerene and Nonfullerene Solar Cells. *J. Phys. Chem. C* **2018**, 122, 16613−16623.

[29] Liu, L.; Li, F.; Wu, C.; Tang, T.; Chen, X.; Luo, X.; Li, J. Synthesis and Properties of Benzodithiophene-Based Donor-Acceptor Metallo-Supramolecular Polymers. *Macromol Res.* **2019**, 27, 534-542.

[30] Duan, C. H.; Gao, K.; Colberts, F. J. M.; Liu, F.; Meskers, S. C. J.; Wienk, M. M.; Janssen, R. A. J. Thiophene Rings Improve the Device Performance of Conjugated Polymers in Polymer Solar Cells with Thick Active Layers. *Adv. Energy Mater.* **2017**, 7, 1700519.

[31] Zhang, Y.; Xu, Y.; Ford, M. J.; Li, F.; Sun, J.; Ling, X.; Wang, Y.; Gu, J.; Yuan, J.; Ma, W. Thermally Stable All-Polymer Solar Cells with High Tolerance on Blend Ratios. *Adv. Energy Mater.* **2018**, 8, 1800029.

[32] Welch, G. C.; Perez, L. A.; Hoven, C. V.; Zhang, Y.; Dang, X.-D.; Sharenko, A.; Toney, M. F.; Kramer, E. J.; Nguyen, T.-Q.; Bazan, G. C. A modular molecular framework for utility in small-molecule solution-processed organic photovoltaic devices. *J. Mater. Chem.* **2011**, 21, 12700–12709.

[33] Kim, J.-H.; Song, C. E.; Shin, N.; Kang, H.; Wood, S.; Kang, I.- N.; Kim, B. J.; Kim, B. S.; Kim, J.-S.; Shin, W. S.; Hwang, D.-H. High-Crystalline Medium-Band-Gap Polymers Consisting of Benzodithiophene and Benzotriazole Derivatives for Organic Photovoltaic Cells. *ACS Appl. Mater. Interfaces* **2013**, 5, 12820−12831.

[34] Kim, J. H.; Wood, S.; Park, J. B.; Wade, J.; Song, M.; Yoon, S. C.; Jung, I. H.; Kim, J. S.; Hwang, D. H. Optimization and Analysis of Conjugated Polymer Side Chains for High-Performance Organic Photovoltaic Cells. *Adv. Funct. Mater.* **2016**, 26, 1517−1525.

[35] Wood, S.; Kim, J.-H.; Hwang, D.-H.; Kim, J.-S. Effects of Fluorination and Side Chain Branching on Molecular Conformation and Photovoltaic Performance of Donor−Acceptor Copolymers. *Chem. Mater.* **2015**, 27, 4196−4204.

[36] Razzell-Hollis, J.; Fleischli, F.; Jahnke, A. A.; Stingelin, N.; Seferos, D. S.; Kim, J.-S. J. Effects of Side-Chain Length and Shape on Polytellurophene Molecular Order and Blend Morphology *Phys. Chem. C* **2017**, 121, 2088−2098

[37] Yu, S. H.; Park, K. H.; Kim, Y.-H.; Chung, D. S.; Kwon, S.-K. Fine molecular tuning of diketopyrrolopyrrole-based polymer semiconductors for efficient charge transport: effects of intramolecular conjugation structure. *Macromolecules* **2017**, 50, 4227 −4234

[38] Li, P.; Wang, G.; Cai, L.; Ding, B.; Zhou, D.; Hu, Y.; Zhang, Y.; Xiang, J.; Wan, K.; Chen, L.; Alameh, K.; Song, Q. High-Efficiency Inverted Polymer Solar Cells Controlled by the Thickness of Polyethylenimine Ethoxylated (PEIE) Interfacial Layers. *Phys. Chem. Chem. Phys.* **2014**, 16, 23792−23799.

[39] Zhou, Y.; Fuentes-Hernandez, C.; Shim, J.; Meyer, J.; Giordano, A. J.; Li, H.; Winget, P.; Papadopoulos, T.; Cheun, H.; Kim, J.; Fenoll, M.; Dindar, A.; Haske, W.; Najafabadi, E.; Khan, T. M.; Sojoudi, H.; Barlow, S.; Graham, S.; Bredas, J.-L.; Marder, S. R.; Kahn, A.; Kippelen, B. Universal Method to Produce Low−Work Function Electrodes for Organic Electronics. *Science* **2012**, 336, 327−332

[40] Zang, Z.; Yu, J.; Yin, X.; Hu, Z.; Jiang, Y.; Sun, J.; Zhou, J.; Zhang, F.; Russell, T. P.; Liu, F.; Tang, W. Conformation Locking on Fused-Ring Electron Acceptor for High-performance Nonfullerene Organic Solar Cell. *Adv. Funct. Mater.* **2018**, 1705095

[41] Nicolai, H. T.; Wetzelaer, G. A. H.; Kuik, M.; Kronemeijer, A. J.; de Boer, B.; Blom, P. W. M. Space-Charge-Limited Hole Current in Poly(9,9-dioctylfluorene) Diodes. *Appl. Phys. Lett.* **2010**, 96, 172107.

[42] Reusch, D.; Strydom, J.; Lidow, A.; A New Family of GaN Transistors for Highly Efficient High Frequency DC-DC Converters. *IEEE.* **2015**, 1979-1985.

요 약 문

넓은 선형 동적범위를 가진 고성능 유기물 광다이오드: 결정 방향의 역할

본 논문은 새로운 고분자 반도체를 이용하여 넓은 선형 동적범위를 구현하는 유기물 광다이오드 개발을 구현한다. alkylthio-substituted benzo[1,2-b:4,5-b’]dithiophene (BDT]를 기반으로 하는 공중 합체 고분자는 fluorinated terthiophene (BDT-Th-3T] 또는 alkylterthiophene (BDT-Th-3AT]와 합성한 새로운 고분자이다. 이 공중합체 고분자들은 2D-GIXD 분석결과에서 알 수 있듯이 ITO/PEIE 기판 위에서 뚜렷한 face-on 배열 방향을 보였으며 특히, BDT-Th-3T 박막은 향상된 결정성을 보였다. 이는 UV-vis-NIR 흡광 분석과 라만 분광학 분석으로부터 알 수 있듯이 BDT-Th-3T의 분자구조의 평면성으평부터 유도되는 비동분자 내 상호작용 및 작은 입체 방해효과의 영향이다. BDT-Th-3T 고분자는 non-fullerene 전자 받개와 혼합되어서도 결정성이 효율적으로 유지되었으며 전자 받개와 전자 주개 모두 수직 구조의 디바이스에서 선호하는 face-on 구조로 형성되어 전하 이동에 유리한 면을 보였다. 그 결과, 최적화된 유기물 광다이오드는 10^{13} jones 가 넘는 높은 검출능과 232dB 의 매우 높은 선형 동적범위를 구현하였다. 이 연구 결과는 차세대 이미지 센서의 유기물 반도체 적용에 있어 더욱 넓은 범위의 이미지 센서 적용에 도움이 될 것이다.

핵심어: 유기물 광다이오드, 선형 동적범위, 광전자 디바이스, 박막, 전하 이동도